CrystEngComm

HIGHLIGHT

View Article Online
View Journal | View Issue

Cite this: *CrystEngComm*, 2016, **18**, 193

Metal–organic frameworks based luminescent materials for nitroaromatics sensing

Liangliang Zhang,† Zixi Kang,† Xuelian Xin and Daofeng Sun*

Received 28th September 2015,
Accepted 30th October 2015

DOI: 10.1039/c5ce01917f

www.rsc.org/crystengcomm

Metal–organic frameworks (MOFs), composed of organic ligands and metal nodes, are well known for their high and permanent porosity, crystalline nature and versatile potential applications, which promoted them to be one of the most rapidly developing research focuses in chemical and materials science. During the various applications of MOFs, the photoluminescence properties of MOFs have received growing attention, especially for nitroaromatics (NACs) sensing, due to the consideration of homeland security, environmental cleaning and military issues. In this highlight, we summarize the progress in recent research in NACs sensing based on LMOFs cataloged by sensing techniques in the past three years, and then we describe the sensing applications for nano-MOF type materials and MOF film, together with MOF film applications.

Introduction

With the increasing use of explosive materials in terrorism all over the world, how to reliably and efficiently detect traces of explosive materials has become a highlighted research focus in recent years because of homeland security, environmental cleaning and military issues.[1] In addition, the reliable identification of chemical explosives in post-blast residues is of great importance for criminal investigations.[1d,2] As one of the major classes of secondary explosives, nitroaromatics (NACs), which are composed of a benzene ring functionalized with several nitro-groups, such as 2,4,6-trinitrotoluene (TNT), 2,4-dinitrotoluene (2,4-DNT) and picric acid (PA), have become serious pollution sources of groundwater, soils, and other security applications due to their explosivity and high toxicity (Fig. 1). Detection of this class of explosives is not easy because of their moderate vapor pressures and limited chemical reactivity.[1e] Thanks to the development of instrumental techniques, together with sniffer dogs,[3] new ways to detect explosives are being developed to improve security, including gas chromatography coupled with mass spectrometry (GC-MS), surface-enhanced Raman spectroscopy, neutron activation analysis, X-ray imaging, ion mobility spectroscopy (IMS), energy dispersive X-ray diffraction (EDXRD), and plasma desorption mass spectrometry (PDMS).[1k,4] These techniques are highly selective and sensitive, but some are of high cost and time-consuming; simultaneously, others are not easy to operate and assemble in a small and low-power package. Therefore, another new technology needs to be

State Key Laboratory of Heavy Oil Processing, China University of Petroleum (East China), College of Science, China University of Petroleum (East China), Qingdao Shandong 266580, People's Republic of China. E-mail: dfsun@upc.edu.cn
† These two authors provided equal contribution to this work.

Liangliang Zhang

Liangliang Zhang completed his PhD in Inorganic Chemistry under the supervision of Prof. Daofeng Sun from Shandong University (2013). He is now a full-time scientific staff member in China University of Petroleum (EastChina). His research interest is focused on the preparation of functional metal–organic frameworks.

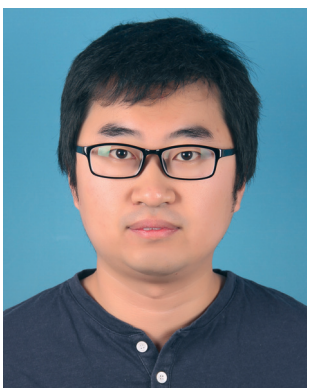

Zixi Kang

Zixi Kang received his BS (2008) and PhD (2013) degrees in Chemistry from Jilin University in China, and joined the National University of Singapore as a post-doc research fellow during 2014–2015. Currently, he works in the College of Science, China University of Petroleum (EastChina), as a lecturer. His work is focused on multifunctional metal–organic framework materials and membranes for applications in adsorption and separation.

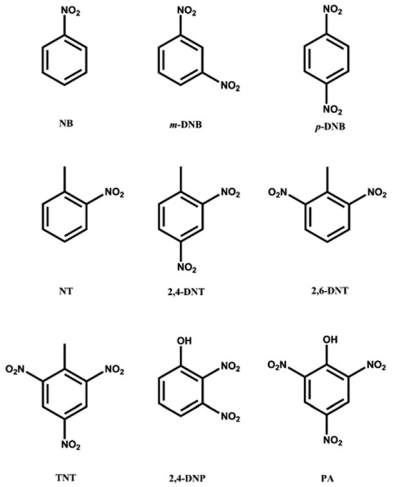

Fig. 1 Chemical structures of common NAC molecules.[1f]

developed so that we may inexpensively and rapidly complete detection. The electron-deficient particular property of NACs is favorable for forming π-stacking complexes with electron-rich fluorophores, which can be applied to their detection with chromo-fluorogenic probes. Chemical sensors provide new approaches to the rapid detection of ultra-trace NACs from explosives, and can be easily incorporated into inexpensive and portable microelectronic devices. In this respect, the fluorescence-based sensor schemes probably show a very promising future.

All sorts of conjugated polymers (CPs) have been used to sense NACs with high sensitivity and selectivity, due to their π-electron-rich characteristic and high binding strength to NACs.[1i,5] The delocalized π* excited state of CPs can significantly enhance their donor ability and enable them to interact strongly with nitrated aromatic compounds through π–π interactions. However, the applications of conjugated polymeric sensors are limited by their instability, multi-step synthesis requirements and poor molecular organization. In addition, it has also been noted that porosity may play an important role in sensing performance, as illustrated in porous amplifying fluorescent polymer (AFP) films, metalloporphyrin-doped mesostructured films and fluorescent nanofibril films.

Metal–organic frameworks (MOFs) materials, constructed from multi-topic organic ligands and metal cations or clusters, have been studied extensively during the past decade for their intriguing structural diversity and potential applications, including selective gas adsorption and separation,[6] catalysis,[7] luminescent sensing[3a,8] and drug delivery.[9] MOFs have become one of the most rapidly developing research focuses in chemical and materials sciences. The most attractive features of MOFs are their high and permanent porosity, long range order, high surface area, as well as uniform pore sizes in the nanoscale range. In addition, their chemical versatility and structural tailorability provide a significant level of tenability to the physical and chemical properties of MOFs. The judicious combination of metal ions and predesigned organic ligands under suitable reaction conditions affords various types of MOF structures with desired functionalities.[10] The luminescence of MOFs originates from the rigid ligands with aromatic moieties or extended π systems and/or metal components, especially for lanthanides and inorganic clusters, excimer and exciplex, or guest molecules. Compared with free organic ligand, the advantages of using MOFs as sensory materials are as follows. First, MOFs in solid may reduce the non-radiative decay rate and leads to increased fluorescence intensity, lifetimes, and quantum efficiencies. In addition, the multifunction of MOFs can easily be modulated by post-synthetic modification and it is supposed that unsaturated metal centers or open metal sites plays important part in absorption/separation including gas and guest molecules. Most notably, the sustainable pores within LMOFs provide a natural habitat for guest molecules. The combination of porosity and luminescence in MOFs makes them potential candidates for the sensing of NACs. Since being reported by Li in 2009, fluorescence based sensing materials have been considered as one of the most excellent and promising techniques in the detection of NACs.[1c]

Xuelian Xin

Xuelian Xin received her MS degree from Jiangsu Normal University in 2014. She is currently a doctoral student under the supervision of Professor Daofeng Sun. Her actual research interest involves the design of luminescent metal–organic framework materials for fluorescent sensors.

Daofeng Sun

Daofeng Sun completed his PhD in Physical Chemistry under the supervision of Prof. Maochun Hong and Rong Cao from Fujian Institute of Research on the Structure of Matter, Chinese Academy of Science (2003). He worked with Prof. Hongcai Zhou at University of Miami, as the postdoctoral fellow during 2003–2006 before joining Shandong University in 2007. He moved to China University of Petroleum (EastChina) in January 2013, and now he is a full professor of Chemistry. His research interests focus on porous materials.

The possible mechanisms of luminescent MOFs for sensing NACs are based on fluorescence quenching, including an electron transfer or energy transfer process, or a combination of the two, between fluorophore and NACs; similar physical processes have been investigated in conjugated polymers.[2,3c,11] The fluorescence quenching mechanism based on electron transfer can also be divided into static quenching and dynamic quenching. Static quenching takes place in the ground-state *via* non-fluorescent electron-transfer complex formation, which decreases the intensity of steady-state emission, without changing the life-time of LMOFs. On the contrary, the dynamic quenching occurs in the excited state *via* an electron-transfer process, which decreases the steady-state emission intensity and life-time of LMOFs simultaneously. As mentioned above, NACs are electron-deficient analytes and LMOFs can be regarded as electron-rich fluorophore molecules whose valence and conduction bands can be treated in a way similar to molecular orbitals (MOs). The vapor pressure of common explosives is listed in Table 1. The electronic properties of LMOFs and NACs are equally important for efficient sensing. In general, the conduction of a LMOF lies at higher energies than the LUMOs of NACs, and thus maintains a better driving force for the electron transfer to electron-deficient NACs, leading to fluorescence quenching. Stern–Volmer analysis can be used to quantitatively evaluate the efficiency of particular LMOFs for NACs in liquid medium using eqn (1).

$$I_o/I_F = 1 + k_{sv}[Q] \quad (1)$$

where I_o and I_f are the fluorescence intensities of LMOFs before and after the addition of NACs. k_{sv} is the Stern–Volmer constant and $[Q]$ stands for the concentration of NACs. A higher k_{sv} means higher sensing efficiency. However, electron transfer is not the sole mechanism: the fluorescence quenching mechanism sometimes originates from the case of energy transfer or the combination of electron and energy transfer. If the emission band of the LMOFs and the absorption band of the NACs are overlapped efficiently, the energy transfer process may occur and will markedly improve the fluorescence quenching efficiency and sensibility. The probability of resonance energy transfer depends on the extent of spectral overlap between the emission of LMOFs and the absorption of NACs. The extent of energy transfer was determined by calculating the integral of overlap (J_λ) values using eqn (2),[12] where $F_D(\lambda)$ is the corrected fluorescence intensity of the donor in the range of λ–$\lambda + \Delta\lambda$, with the total intensity normalized to unity, and ε_A is the extinction coefficient of the acceptor at λ in M^{-1} cm^{-1}.

$$J(\lambda) = \int_0^\infty F_D(\lambda)\varepsilon_A(\lambda)\lambda^4 d\lambda \quad (2)$$

The advantages and challenges of LMOFs-based chemical sensing and explosive detection have been well summarized by recent review articles.[1f,8b,c,11,13] Our research interest focusses on NACs sensing based on LMOFs. In this highlight, we summarize the recent research progress in NACs sensing based on LMOFs cataloged using sensing technique in the past three years (Table 2), and then we describe the sensing applications of nano-MOF type materials and MOF film, together with MOF film applications.

Table 1 The vapor pressure of common NACs

Analyte	Vapor pressure (in mmHg,[a] at 25 °C)
Nitrobenzene (NB)	0.2416
1,3-Dinitrobenzene (*m*-DNB)	8.82×10^{-4}
1,4-Dinitrobenzene (*p*-DNB)	2.406×10^{-5}
2-Nitrotoluene (NT)	0.1602
2,4-Dinitrotoluene (2,4-DNT)	1.44×10^{-6}
2,6-Dinitrotoluene (2,6-DNT)	5.61×10^{-4}
2,4,6-Trinitrotoluene (TNT)	8.02×10^{-6}
Picric acid (PA)	5.8×10^{-9}

[a] 1 mmHg = 1.2468×10^3 ppm.

2 MOFs for NACs sensor

As a new frontier for material research, metal–organic frameworks (MOFs) have gathered much attention in the past decades due to their multi-functional applications. A brand new field of MOF research associated with the detection of NACs was presented after first being reported by Li *et al.* Among the reported studies, MOFs or hybrid MOFs were applied for the detection of NACs with high selectivity and sensitivity in the vapor phase, liquid phase and/or aqueous phase. The results show that LMOFs are promising materials for tracing nitroaromatic explosives.

2.1 Detection in vapor phase

Gas sensors have a wide range of application in the fields of aerodynamics, environmental analysis, analytical chemistry, and biochemistry. As the luminescent properties of MOFs can also be perturbed by gases and vapors, some luminescent MOFs for sensing gases and vapors have also been explored.[3a,11] The very first MOF used as sensor in the vapor phase to detect NACs explosives was reported by Li's group.[1c] They designed and synthesized a fluorescent MOF, $[Zn_2(bpdc)_2(bpee)]\cdot 2DMF$ (bpdc = 4,4′-biphenyldicarboxylate; bpee = 1,2-bipyridylethene; DMF = dimethyl formamide). The MOF consisted of 1D open channels, in which DMF molecules were filled in, and the solvent molecules could be removed by heating under vacuum to obtain the guest-free MOF. The guest-free MOF showed strong fluorescence in solid state. To explore the applicability for the detection of NACs, the guest-free MOF was made as a thin layer. The sample showed rapid and reversible response to DNT vapor, the quenching percentage reached 85% within 10 seconds. Thus, it is important that the samples can detect DNT circularly by heating the samples at 150 °C for one minute. Moreover, Li's group also reported a Zn based LMOF, LMOF-121 or $[Zn_2(oba)_2(bpy)]\cdot 3DMA$, H_2oba = 4,4′-oxybis(benzoic acid), bpy = 4,4′-bipyridine, DMA = *N*,*N*′-dimethylacetamide.[1g] As shown in Fig. 2, LMOF-121 possessed a 3D network built from a

Table 2 List of selected LMOFs from the past three years

LMOFs	Solvent	Sensing technique	λ_{ex} (nm)	λ_{em} (nm)	Ref.
$[Zn(L^1)(dpb)]$	EtOH	Liquid phase	310	415	14
$[Zn(L^2)(dpb)]$	EtOH	Liquid phase	300	420	14
$[Zn(L^3)(dpb)]$	EtOH	Liquid phase	360	480	14
$[Zn_2(NDC)_2(bpy)]\cdot G_x$	EtOH	Liquid phase	320	450	1*m*
$Zn(L^4)\cdot(HDMA)_2(DMF)(H_2O)_6$	EtOH	Liquid phase	Not given	475	15
$\{[Zn_2(PIA)_2(bpy)_2]\cdot 2.5H_2O\cdot DMA\}_n$	EtOH	Liquid phase	280	326	16
$[\{Cd(fdc)(bpee)_{1.5}\}\cdot 3(H_2O)]$	EtOH	Liquid phase	300	425	17
$[Cd_3(CPEIP)_2(DMF)_3]\cdot$solvent	EtOH	Liquid phase	342	Not given	18
$[Cd_2Cl(tba)_3]\cdot 0.5DMF\cdot 2H_2O$	EtOH	Liquid phase	323	381	19
$[Cd_3(TPT)_2(DMF)_2]\cdot(H_2O)_{0.5}$	EtOH	Liquid phase	333	390	20
$[La(TPT)(DMSO)_2]\cdot H_2O$	EtOH	Liquid phase	342	374	21
$Eu_2(BDC)_3(H_2O)_2$	EtOH	Liquid phase	315	617	22
$[Tb(HL^5)(H_2O)_4]\cdot H_2O$	EtOH	Liquid phase	288	546	23
$\{[Tb_2(TATAB)_2]\cdot 4H_2O\cdot 6DMF\}_n$	EtOH	Liquid phase	350	545	24
Tb(BTC)	EtOH	Liquid phase	353	548	25
$[Tb(TTCA)(DMA)(H_2O)]\cdot 7DMA\cdot 9.5H_2O$	EtOH	Liquid phase	370	540	26
$[Zn_2(L^1)(L^2)(dpb)_2]$	EtOH	Liquid phase	330	417	27
$[Zn_2(L^1)(L^3)(dpb)_2]$	EtOH	Liquid phase	347	471	27
$[Zn_2(L^2)(L^3)(dpb)_2]$	EtOH	Liquid phase	350	476	27
$[Zn_3(L^1)(L^2)(L^3)(dpb)_3]$	EtOH	Liquid phase	350	473	27
$[Zn_3(TDPAT)(H_2O)_3]$	MeOH	Liquid phase	370	435	28
$[Zn_4(OH)_2(1,2,4\text{-}BTC)_2]$	MeOH	Liquid phase	331	428	29
$[Zn_4O(L^6)_3(DMF)_2]\cdot 0.5DMF\cdot H_2O$	MeOH	Liquid phase	280	380	30
$(NH_2Me_2)_6[In_{10}(TTCA)_{12}]\cdot 24DMF\cdot 15H_2O$	MeOH	Liquid phase	410	505	31
[Zn(PAM)(en)]	DMSO	Liquid phase	371	503	32
$[Cd_2(PAM)_2(dpe)_2(H_2O)_2]\cdot 0.5(dpe)$	DMSO	Liquid phase	371	502	33
$[Eu(L^7)(H_2O)(NMP)]\cdot 1.5H_2O$	DMSO	Liquid phase	298	616	34
$[Tb_3(NO_3)(BPTA)_2(H_2O)_6]\cdot 3Diox\cdot 8H_2O$	DMSO	Liquid phase	330	545	1*l*
$\{Li_3[Li(DMF)_2](CPMA)_2\}\cdot 4DMF\cdot H_2O$	DMF	Liquid phase	345	430	35
$[NH_2(CH_3)_2][Mg_3(NDC)_{2.5}(HCO_2)_2(DMF)_{0.75}(H_2O)_{0.25}]$ 1.25DMF 0.75H2O(H2O)0.25] ═1.25DMF═ 0.75H2O	DMF	Liquid phase	340	380	36
$[Zn_7O_2(bpdc)4(dmpp)2]\cdot 6DEF\cdot 10H_2O$	DMF	Liquid phase	323	390	37
$[Zn_2(bpeb)(sdb)_2]$	DMF	Liquid phase	360	453	38
$[Zn_2(fdc)_2(bpee)_2(H_2O)]_n\cdot 2H_2O$	DMF	Liquid phase	350	425	39
$[(Zn_4O)(DCPB)_3]\cdot 11DMF\cdot 5H_2O$	DMF	Liquid phase	330	354	40
$[(CH_3)_2NH_2][Zn_3(HL^8)(H_2O)_2]\cdot 4H_2O$	DMF	Liquid phase	374	443	41
$[NH_2Me_2]_4[Cd_3(H_2L^9)]$	DMF	Liquid phase	348	446	42
$[Cd_5(TCA)_4(H_2O)_2]$	DMF	Liquid phase	352	417	43
$[NH_2(CH_3)_2]_2[Cd_{17}(L^{10})_{12}(H_2O)_4(DMF)_2(H_2O)_2]$	DMF	Liquid phase	290	360	44
$[Cd_8(D\text{-}cam)_8(bimb)_4]_n$	DMF	Liquid phase	370	410	45
$[Cd(TPTZ)(H_2O)_2(HCOOH)(IPA)_2]_n$	DMF	Liquid phase	360	450	46
$[Cd_3(TTPB)_2(H_2O)_6]\cdot 6DMF$	DMF	Liquid phase	366	440	47
$[NH_2(CH_3)_2][Cd_6(L^{10})_4(DMF)_6(HCOO)]$	DMF	Liquid phase	290	353	48
$Eu_3(MFDA)_4(NO_3)(DMF)_3$	DMF	Liquid phase	336	615	49
$(Me_2NH_2)_3[Eu_3(MHFDA)_4(NO_3)_4(DMF)_2]\cdot 4H_2O\cdot 2MeCN$	DMF	Liquid phase	340	614	50
$[Eu_2(MFDA)_2(HCOO)_2(H_2O)_6]$	DMF	Liquid phase	335	614	51
$[Ln(L^{11})_{1.5}(DEF)]_n$	DMF	Liquid phase	340	615	52
$[In_2L^{12}][NH_2(CH_3)_2]_2\cdot(DMF)_4(H_2O)_{16}$	DMF	Liquid phase	280	360	53
$Cd(L^4)\cdot(NH_2Me_2)_2(DMF)(H_2O)_3$	Acetonitrile	Liquid phase	330	460	15
$Zn(L^4)\cdot(NH_2Me_2)_2(DMF)(H_2O)_6$	Acetonitrile	Liquid phase	330	452	15
$Mg_5(OH)_2(BTEC)_2(H_2O)_4\cdot 11H_2O$	THF	Liquid phase	328	425	54
PCN-224		Liquid phase	590	651	55
$[Zn_2(L^{13})_2(dpyb)]$	DMA	Liquid phase	382	533	56
$[Zn(L^{13})(dipb)]\cdot(H_2O)_2$	DMA	Liquid phase	382	523	56
$\{[Cd_2L^{14}(H_2O)_2]\cdot DMF\cdot H_2O\}_n$	DMA	Liquid phase	290	401	57
$[Cd(L^{15})_{0.5}(H_2O)]\cdot H_2O$	DMA	Liquid phase	350	414	58
$[Cd_2Cl(H_2O)(L^{16})]\cdot 4.5DMA$	DMA	Liquid phase	295	377,390,474	59
$[Cd_3(NTB)_2(DMA)_3]\cdot 2DMA$	DMA	Liquid phase	366	443	60
$[CdCl(L^{17})Eu(H_2O)(DMA)]\cdot(NO_3)\cdot 3DMA$	DMA	Liquid phase	367	671	61
$\{[Zn_3(\mu\text{-}OH)_2(SDB)_2]\cdot(PPZ)\}_n$	Acetone	Liquid phase	270	292	62
$\{[Cd(SDB)(H_2O)]\cdot 3H_2O\}_n$	Acetone	Liquid phase	270	290	62
$[Eu_3(bpydb)_3(HCOO)(OH)_2(DMF)]\cdot(DMF)\cdot 3(H_2O)_2$	DMF and H_2O	Liquid phase	362	615	63
$[Cd(H_2ttac)bpp]_n$	DMF and ethanol	Liquid phase	320	415	64
$[Zn_2(L^{18})(bipy)(H_2O)_2]\cdot(H_2O)_3(DMF)_2$	MeCN	Liquid phase	350	476	65
$Cd(L^4)\cdot(HDMA)_2(DMF)(H_2O)_3$	MeCN	Liquid phase	Not given	460	15
$[Cd(NDC)_{0.5}(PCA)]\cdot G_x$	MeCN	Liquid phase	340	384	12*a*
$[Mg_2(BDC)_2(BPNO)]\cdot 2DMF$		Vapor phase	305	421	66

Table 2 *(continued)*

LMOFs	Solvent	Sensing technique	λ_{ex} (nm)	λ_{em} (nm)	Ref.
$[Zn_{1.5}(L^{19})(H_2O)]\cdot 1.5$benzene		Vapor phase	280	390	67
$[Zn_2(TCPPE)]$		Vapor phase	365	461	68
$[Zn_2(oba)_2(bpy)]\cdot 3DMA$		Vapor phase	280	420	1*g*
$[Zn_2(bpdc)_2(bpee)]\cdot 2DMF$		Vapor phase	320	422	1*c*
$[Zn(ndc)(bpy)_{0.5}]$		Vapor phase	300	450	69
$[Zn(ndc)(bpe)_{0.5}]$		Vapor phase	330	425	69
$[Zn(ndc)(bpee)_{0.5}]$		Vapor phase	330	450	69
$[Zn(ndc)(ted)_{0.5}]$		Vapor phase	340	420	69
$[Zn(dcbpy)(DMF)]\cdot DMF$		Vapor phase	Not given	Not given	70
$[Dy(dcbpy)(DMF)_2(NO_3)]$		Vapor phase	Not given	Not given	70
$[Zn_8(ad)_4(BPDC)_6O\cdot 2Me_2NH_2]\cdot G$(G = DMF and water)	H_2O		340	405	71
$[(CH_3)_2NH_2]_3[Zn_4Na(BPTC)_3]\cdot 4CH_3OH\cdot 2DMF$	H_2O		295	360	72
$[Cd(ppvppa)(1,4\text{-}NDC)]_n$	H_2O		419	478	3*b*
$[Eu(BTB)H_2O]$	H_2O		350	610	73
$\{[Tb(L^{20})_{1.5}(H_2O)]\cdot 3H_2O\}$	H_2O		329	541	74
$[Tb(L^{21})(OH)]\cdot_x$(solv)	H_2O		350	541	75
$[Tb(BTB)H_2O]$	H_2O		350	541	73
$Zr_6O_4(OH)_4(L^{22})_6$	H_2O		395	500	76
$Zr_6O_4(OH)_4(L^{24})_6$	H_2O		320	450	77
Ur-MOF	H_2O		310	390	78

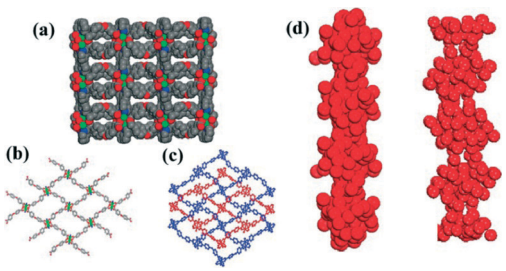

Fig. 2 Crystal structure of $[Zn_2(oba)_2(bpy)]\cdot DMA$. (a) Space-filling model of the 3D framework, showing the 1D channels running along the 100 direction without DMA molecules. (b) A single layer (Zn, green; N, blue; O, red). (c) Two-fold interpenetration, shown by two different colors (blue and red). (d) The atom filling in a single channel along the (left) 010 and (right) 100 direction. Reprinted with permission from ref. 1*g*. Copyright American Chemical Society 2011.

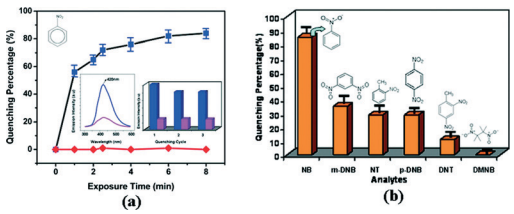

Fig. 3 (a) Time-dependent fluorescence quenching by NB (black line) and DMNB (red line). Insets: (left) corresponding emission spectra before and after exposure of LMOF-121' to the NB vapor; (right) results for three continuous quenching cycles. (b) Percentage of fluorescence quenching after 15 min by five different analytes at room temperature. Reprinted with permission from ref. 1*g*. Copyright American Chemical Society 2011.

$Zn_2(oba)_4$ paddle-wheel SBU. The structure contained one-dimensional open 1D channels running along both the 100 and 010 directions, wherein the DMA molecules resided. To obtain the empty pore for capturing the guest molecule, LMOF-121 was heated at 160 °C to remove DMA molecules, producing LMOF-121'. The fluorescent spectra of LMOF-121' was investigated in a thin layer, which showed strong emission at 420 nm (λ_{ex} = 280 nm). The layer was exposed to different NACs with electron withdrawing groups. The results indicated that all the NACs used in the study acted as fluorescence quenchers. The quenching efficiency (%) of NB was 84%, which was the highest one (Fig. 3). In the vapor phase, the quenching efficiency is not only affected by the strong electron-withdrawing $-NO_2$ group, but also associated with vapor pressure. Recently, the same group reported a series of fluorescence active MOFs built on paddle-wheel secondary building units (SBUs), including $[Zn(ndc)(bpe)_{0.5}]$ (**1**), $[Zn(ndc)(bpee)_{0.5}]$ (**2**), $[Zn(ndc)(ted)_{0.5}]$ (**3**) and $Zn(ndc)(bpy)_{0.5}$ (**4**) [ndc = 2,6-naphthalenedicarboxylic acid; bpe = 1,2-bis(4-pyridyl)ethane; bpee = 1,2-bis(4-pyridyl)ethylene; ted = triethylenediamine, bpy = 4,4′-bipyridine]. All compounds performed luminescence quenching when they were exposed to the NACs vapor. Among them, complex **3** possesses the best quenching ability, with a quenching ratio about 84% and 51% for NB and NT vapor, respectively.[69] Similar results can be observed in Wang,[66] and Shen's[68] study.

LMOFs can also be synthesized *via* a microwave-assisted method because it sharply reduces the over-all processing time, increases the product yield and improves the quality of the product. Compared to their solvothermally synthesized counterparts, microwave-assisted LMOFs with homogenous microcrystals give increased sensing sensitivities. Parkin and coworkers reported two fluorescent metal–organic frameworks $[Zn(dcbpy)(DMF)]\cdot DMF$ (**1**) and $[Dy(dcbpy)(DMF)_2(NO_3)]$ (**2**) (dcbpy = 2,2′-bipyridine-4,4′-dicarboxylate), together with a microwave synthesized form as **1M**. Microporous **1** and non-porous **2** give organic linker-based fluorescence emission. Furthermore, MOFs **1**, **1M** and **2** were tested for their ability to act as sensory materials for TNT derivatives: 2,4-dinitrotoluene

(2,4-DNT), para-nitrotoluene (*p*-NT) and nitrobenzene (NB), as well as plastic explosive taggant 2,3-dimethyl-2,3-dinitrobutane (DMNB) in the vapor phase. They demonstrated very different detection capabilities towards the explosive taggant. Compared with non-homogenous microcrystals of **1′**, **1M** shows greater sensitivities for quenching responses when exposed to DMNB and NB. They believe that the differences are attributed to the variation in the overall framework architecture between the two MOFs. This study reiterates the key importance of MOF porosity in sensing applications, and highlights the value of uniform microcrystals to sensitivity.[70]

2.2 Detection in liquid phase

In recent years, most LMOFs for NACs sensors are detected in an organic liquid phase, including EtOH, MeOH, DMF, DMA, DMSO and MeCN, especially for unstable MOFs. Our group has reported an example of MOFs as an efficient sensor for NACs detection.[34] $[Eu_2(L^7)_2(H_2O)_3]\cdot 2H_2O$ (H_3L^7 = 1,3,5-tris(4-carboxyphenyl-1-ylmethyl)-2,4,6-trimethylbenzene) was crystallized in an orthorhombic space group of *Pnma*. As shown in Fig. 4(a)–(d), the binuclear Eu clusters are connected to each other by two carboxylate groups to form a 1D infinite rod-shaped SBU along the *c* axis. The 1D chain is further linked by ligands to form a porous 3D MOF, which contains a rhombic channel viewed from the *c* axis. The detection of various NACs was tested. The fluorescence quenching percentage was shown in Fig. 4(e) and (f), and the number is up to 75% for NP at a concentration of 0.13 mM in DMSO solution. The results showed that the OH^- group in NP, which apparently possibly interacts with the emission through electrostatic interactions. As a continuance of our study, we also reported a Tb based MOF, $[Tb_3(NO_3)(BPTA)_2(H_2O)_6]\cdot 3diox\cdot 8H_2O$ (**UPC-11**, H_4BPTA = [1,1′-biphenyl]-2,2′,5,5′-tetracarboxylic acid, diox = 1,4-dioxane), which could rapidly and selectively detect NACs. The MOF exhibits luminescent emissions at 290, 545, 584 and 622 nm with the excitation at 330 nm, and those peaks are tentatively assigned to $^5D_4 \rightarrow {}^7F_6$, $^5D^4 \rightarrow {}^7F_5$, $^5D^4 \rightarrow {}^7F_4$, $^5D^4 \rightarrow {}^7F_3$ transitions of Tb^{3+} ion. The luminescence titration showed that all NACs can weaken the fluorescence intensity of a **UPC-11** suspension, but the quenching percentage exhibits a big difference. Moreover, the addition of 1,3-DNB, 2,4-DNT, 1,4-DNB, 4-NA, 1-M-4-NB, and 4-NPH solutions caused a relatively little but similar fluorescence intensity change of suspension, but the introduction of 4-NP produced significant quenching of fluorescence intensity. **UPC-11** shows rapid and selective fluorescence sensing properties of NACs, especially for 4-nitrophenol (NP).[1l]

Nitroaromatic explosives with different numbers of $-NO_2$ groups can be detected qualitatively and quantitatively according to Lan and Su's report.[79] They present a luminescent Ln^{3+}@MOF approach to realize a fast and effective Ln^{3+}@MOF sensor used to detect nitroaromatic explosives with high recyclability through fluorescence quenching. And the concentrations of complete quenching are about 2000, 1000, and 80 ppm for nitro-benzene, 1,3-dinitrobenzene, and 2,4,6-trinitrophenol, respectively. Meanwhile, to examine the sensing sensitivity toward TNP in more detail, a batch of suspensions of Tb^{3+}@NENU-522 were prepared by dispersing it in a DMF solution while gradually increasing the contents to monitor the emissive response. Tb^{3+}@NENU-522 displays high selectivity and recyclability in the detection of nitroaromatic explosives. The group also reported NENU-503 for quick and sensitive detection of nitroaromatic explosives through fluorescence quenching.[59] Notably, the detection of TNT by the MOF can be easily distinguished by the naked eye (Fig. 5). This fluorescence quenching is ascribed to photo-induced electron transfer and resonance energy transfer. For

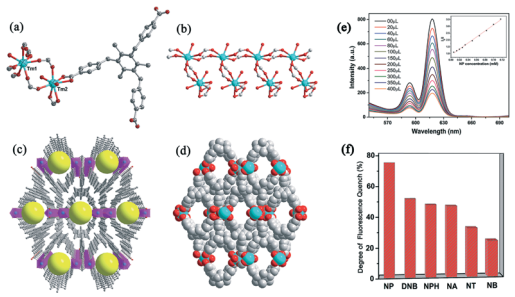

Fig. 4 (a) Coordination environment of Eu atoms in $[Eu_2(L^7)_2(H_2O)_3]\cdot 2H_2O$. (b) The 1D rod shaped SBU in $[Eu_2(L^7)_2(H_2O)_3]\cdot 2H_2O$. (c) Projection view of the framework $[Eu_2(L^7)_2(H_2O)_3]\cdot 2H_2O$ along the *c* axis. (d) 3D porous framework shown in the space-filling mode. (e) Effect on the emission spectra of $[Eu_2(L^7)_2(H_2O)_3]$ dispersed in DMSO upon incremental addition of a NP DMSO solution (1 mM). The legend indicates the overall concentration of NP. The Stern–Volmer plot of I_0/I *versus* the NP concentration is shown in the inset. (f) The degree of fluorescence quenches upon the addition of the nitrobenzene derivatives (0.13 mM). Reprinted with permission from ref. 34. Copyright the Royal Society of Chemistry 2015

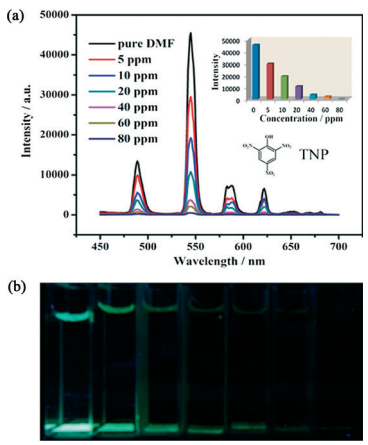

Fig. 5 (a) Emission spectra of Tb^{3+}@NENU-522 in different concentrations TNP in DMF (excited at 333 nm). Inset: corresponding emission intensities. (b) Corresponding emission intensities of Tb^{3+}@NENU-522 in different concentrations of TNP in DMF. Reprinted with permission from ref. 59. Copyright American Chemical Society 2015.

the first time, a MOF can distinguish between NB, 1,3-DNB, and TNP with different numbers of NO_2 groups by the shift of the PL spectra. High stability and recyclability of NENU-503 make it an outstanding candidate in the field of detection of explosives.

2.3 Detection in both vapor and solution phase

The detection of NACs can also be operated in both the vapor and the solution phase. Lu's group reported a 3D luminescent microporous MOF with 1D channels based on triphenylene-2,6,10-tricarboxylate, $(Me_2NH_2)_6[In_{10}(TTCA)_{12}]\cdot 24DMF\cdot 15H_2O$ (TTCA = triphenylene-2,6,10-tricarboxylate and DMF = *N*,*N*′-dimethylformamide).[31] The framework is anionic and Me_2NH^{2+} cations decomposed from DMF are filled in the channels to balance the charge. The photoluminescence spectrum of the framework exhibits strong emission at 505 nm with excitation at 410 nm. The maximum fluorescence intensity of the sample was reduced by 41.7%, 62.1%, 73.5%, and 65.9% upon exposure to 2 mM methanol solutions of TNT, 2,4-DNT, 2,6-DNT, and NB, respectively. The compound shows selective sensing of the nitro explosive TNP, making it a promising sensing material for TNP monitoring.

Chen's group developed a fluorescent In based MOF, $[In_2L^{12}][NH_2(CH_3)_2]_2\cdot(DMF)_4(H_2O)_{16}$ (DMF = *N*,*N*′-dimethylformide, H_8L^{12} = tetrakis[(3,5-dicarboxyphenoxy)methyl]-methane with a (4,8)-connected *scu* topology (Fig. 6). $[In_2L^{12}][NH_2(CH_3)_2]_2\cdot(DMF)_4(H_2O)_{16}$ exhibited a strong fluorescent emission at 360 nm (λ_{ex} = 280 nm) at room temperature. On one hand, in the vapor phase, the MOF dispersed in DMF was exposed to different concentrations (mol L^{-1}) of several NACs. The fluorescence intensity reduced by 81.5% of 5×10^{-6} mol L^{-1} NB is the most efficient (Fig. 7). The excellent fluorescence quenching response to NACs is due to the electrostatic interactions between the MOF and the electron-deficient NACs. The quenching response is associated with both the electron-withdrawing groups of NACs and the sizes of the pores in MOF. On the other hand, the samples were immersed in DMF solution and several analytes (0.5 mol L^{-1}) were added into the solution. The NACs show inefficient quenching, and the quenching mechanism is similar to those previously reported by Li's group.[53]

In Zhang's study, a multi-responsive sensor with a red-emission signal is successfully obtained by the solvothermal

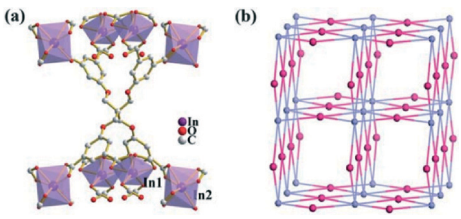

Fig. 6 Views of (a) the organic ligand, which is connected to eight In atoms; (b) the resulting 4,8-connected framework with *scu* topology. Reprinted with permission from ref. 53. Copyright the Royal Society of Chemistry 2013.

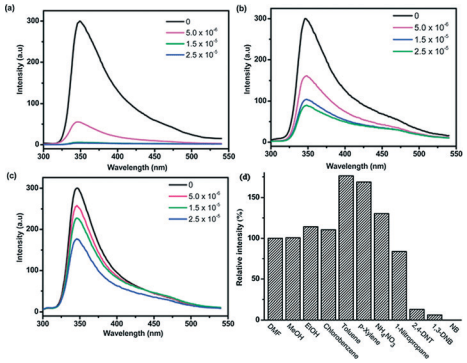

Fig. 7 Quenching response before and after exposure to different concentrations (mol L^{-1}) of (a) NB, (b) 1,3-DNB, and (c) 2,4-DNT in DMF solution for 2 min (λ_{ex} = 280 nm). (d) Percentage of fluorescence quenching or enhancement after the samples were immersed in different analytes (0.5 mol L^{-1}) in DMF for 2 min at room temperature (excited at 280 nm). Reprinted with permission from ref. 53. Copyright The Royal Society of Chemistry 2013.

reaction of Eu^{3+} and heterofunctional ligand $bpydbH_2$ (4,4′-(4,4′-bipyridine-2,6-diyl)dibenzoic acid), followed by terminal-ligand exchange in a single-crystal-to-single-crystal transformation. It can discriminate among the homologues and isomers of aliphatic alcohols and detect highly explosive 2,4,6-trinitrophenol (TNP) in water or in the vapor phase, which may be attributed to the electrostatic interactions between free Lewis-base sites and hydroxyl groups in analytes.[63]

Konar and coworkers reported a 2D Cu(I)-based MOF, $[Cu(I)(I)]_{2n}\cdot 2n$DMF·nMeCN (**1**) (L^{23} = 4′-(4-methoxyphenyl)-4,2′:6′,4″-terpyridine; DMF = *N*,*N*′-dimethylformamide, MeCN = acetonitrile) (Fig. 8), which seems to be the first report of any material that reversibly encapsulates explosive nitroaromatics in the vapor phase in single crystal to single crystal fashion with visible color changes without loss of framework integrity (Fig. 9). The MOF also represents one of the best hosts reported so far having extreme stability and selectivity that meets the benchmark of reversibility for material applications.[80]

Hou and Zang have reported a highly fluorescent MOF {[Tb(L^{21}) (OH)]·x(solv)} under a combination of hydro/solvothermal and ionothermal conditions.[75] The fluorescence of that MOF shows high selectivity and sensitivity towards

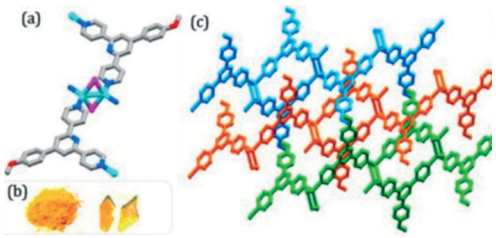

Fig. 8 (a) Illustration of $[Cu_2L^{23}{}_2]$ as a secondary building unit (SBU) and its extension through ligands (L^{23}). (b) Color of the powder form and crystals of the as-synthesized complex. (c) 3D interdigitated structure showing three neighboring layers in three different colors. Reprinted with permission from ref. 80. Copyright the American Chemical Society 2015.

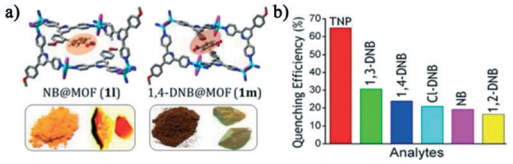

Fig. 9 (a) Illustration of guest exchange with visible color changes in NB and 1,4-DNB vapors. (b) Fluorescence quenching efficiency for different analytes in MeCN solution. Reprinted with permission from ref. 80. Copyright the American Chemical Society 2015.

the presence of trace amounts of nitroaromatic analytes in both aqueous and vapor phases, probably through a redox quenching mechanism similar to that in conjugated polymer systems. The origin of the highly selective sensing towards nitroaromatic explosives can be attributed to a photo-induced electron transfer from MOF to nitroaromatic explosives. Further analysis demonstrates that TNP can efficiently quench the fluorescence of the MOF *via* both electron and long range energy transfer processes, whereas other nitroaromatic explosives quench the fluorescence by an electron transfer process only.

2.4 Detection in aqueous phase

In actuality, the detection of nitroaromatics in an aquatic system is highly desirable for practical applications. Ghosh reported a fluorescent porous Zr(IV) based MOF $Zr_6O_4(OH)_4(L^{24})_6$ (**1**, UiO-67@N, H_2L^{24} = 2-phenylpyridine-5,4′-dicarboxylic acid) that demonstrated highly selective and sensitive detection of TNP in aqueous media even in the presence of competing nitro analytes (Fig. 10).[77] The guest free MOF was dispersed in water and exhibited strong fluorescence upon excitation at 320 nm. Ghosh explored the changes of fluorescence intensity when different nitro aromatic compounds, such as TNP, TNT, 2,4-DNT, 2,6-dinitrotoluene (2,6-DNT), 1,3-dinitrobenzene (DNB), NB and 1,3,5-trinitro-1,3,5-triazacyclohexane (nitro-amine RDX), were added. Incremental addition of TNP to **1′** resulted in fast and high fluorescence quenching (73%) (Fig. 11). Fluorescence quenching can be clearly observed for TNP concentrations as low as 2.6 mM. At low TNP concentrations a linear increase in the SV plot was observed, and the fitting of the SV plot for TNP, gave a quenching constant of 2.9×10^4 M^{-1}, which is amongst the highest values known for MOFs. The occurrence of both electron and energy transfer processes, in

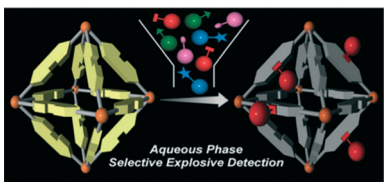

Fig. 10 A fluorescent MOF based sensor for highly selective nitro explosive detection in the aqueous phase. Reprinted with permission from ref. 77. Copyright the Royal Society of Chemistry 2014.

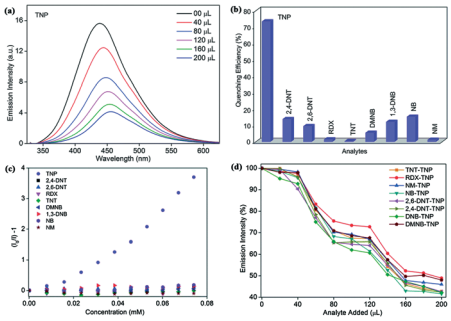

Fig. 11 (a) The change in the fluorescence intensity in water upon increasing addition of aqueous 1 mM TNP solution (λ_{ex} = 320). (b) The fluorescence quenching efficiency for different analytes; (c) Stern–Volmer (SV) plots for various NACs in water. (d) The decrease in fluorescence intensities upon the addition of various nitro analytes (1 mM) followed by TNP (1 mM) in aqueous media. Reprinted with permission from ref. 77. Copyright The Royal Society of Chemistry 2014.

addition to electrostatic interaction between the MOF and TNP, contributes to the unprecedented selective fluorescence quenching.[77] They also reported a hydrolytically stable 3D luminescent metal–organic framework, $[Zn_8(ad)_4(BPDC)_6O \cdot 2Me_2NH_2]\cdot G$ (G = DMF and water). The compound in water exhibited a strong emission at 405 nm (λ_{ex} = 340 nm). The emission spectra were obtained by fluorescence titration with different NACs such as TNP, TNT, 2,4-DNT, and 2,6-DNT. The results showed fast detection and high fluorescence quenching (93%) for TNP. The MOF can sense TNP at extremely low concentrations, with a detection limit of 12.9 nM.[71] Recently, the same group developed a highly selective and sensitive aqueous phase detection of NACs such as 2,4,6-trinitrophenol (TNP) by a water-stable, porous luminescent metal–organic framework, $[Zn_4(DMF)(Ur)_2(NDC)_4]$ (NDC = 2,6-naphthalenedicarboxylic acid, Ur = urotropin, DMF = *N*, *N*′-dimethylformamide).[78]

Ionic liquids (ILs) assisted synthesis of MOFs have received increasing attention because their strong polarity, which improves the reaction conditions of crystalline materials. Hou and Zang's group reported two novel lanthanide metal–organic frameworks (Ln-MOFs) $[Ln(BTB)H_2O]$ *via* an ionic liquids method, where Ln = Eu **1**, Tb **2**. **1** and **2** are isostructural and consist of infinite rod-shaped lanthanide-carboxylate building units, which are further bridged by trigonal-planar BTB ligands to give non-interpenetrated open 3D frameworks. The fluorescence properties of **1** and **2** were investigated in water emulsions at 293 K. **1** and **2** both show high selectivity and sensitivity towards the presence of trace amounts of nitroaromatic analytes in the aqueous phase. The emission response was monitored by fluorescence titration with NB, TNP, and 2-NT. The fluorescence quenching efficiency of **1** and **2** increased drastically with the analytes (NB, TNP, and 2-NT). The quenching efficiency can be quantitatively explained by the Stern–Volmer equation, and the calculated K_{sv} values for NB, 2-NT, and TNP were 6.17×10^{-2}, 2.87×10^{-2}, and 6.76×10^{-2} ppm^{-1} for **1**, and 7.54×10^{-2},

7.46×10^{-2}, and 3.25×10^{-2} ppm^{-1} for **2**, respectively. The fluorescence response mechanism might be attributed to photo-induced electron transfer from the excited MOF to the electron-deficient analytes adsorbed on the particle surface of **1** and **2**.[73] Su and Qin's group reported a stable luminescent anionic metal–organic framework $[(CH_3)_2NH_2]_3\{Zn_5Na_2(BPTC)_4\}_n \cdot 4CH_3OH \cdot 2DMF$, which showed highly selective detection of TNP in an aqueous solution, which can be attributed to electron transfer mechanisms as well as energy transfer mechanisms.[72]

2.5 Detection with hybrid MOFs

Qiu *et al.* have reported a rational self-sacrificing template strategy to obtain tubular nanostructures based on MOF-type materials, and have demonstrated their application for trace-level detection of nitroaromatic explosives. The resultant fluorescent MOFNTs have proven fast, highly sensitive and selective, and reversible for trace-level detection of nitroaromatic explosives, clearly demonstrating that such fluorescent tubular MOF nanostructures can serve as an ideal candidate for fast detection of nitro explosives (Fig. 12).[81]

The same group also successfully fabricated $[Tb(BTC)]_n$ nanocrystals by a combined ultrasound-vapor phase diffusion method.[25] The nanoscale Tb-based MOFs exhibit excellent luminescence properties for the highly selective and sensitive detection of PA, and no obvious interference from other nitroaromatic compounds, such as NB, 2-NT, 4-NT, 2,4-DNT and 2,6-DNT, or common organic solvents, was observed.

Qiu's group also tried to combine MOFs with other materials for detection of explosives.[82] They present novel types of Fe_3O_4@Tb-BTC magnetic MOF nanospheres, which possess both magnetic characteristics and fluorescent properties using a layer by layer assembly technique. It was applied in the detection of nitroaromatic explosives such as 2,4-dinitrotoluene (2,4-DNT), 2,6-dinitrotoluene (2,6-DNT), 2-nitrotoluene (2-NT), 4-nitrotoluene (4-NT), nitrobenzene (NB) and picric acid (PA). The results indicate that the fluorescence intensity of Fe_3O_4@Tb-BTC can be quenched by all analytes studied in the present study (Fig. 13). Remarkably, the as-synthesized nanospheres exhibit high sensitivity for 2,4,6-trinitrotoluene (TNT) detection with a K_{sv} value of (94 800 M^{-1}). In addition, the magnetic nanospheres can be recycled easily, which makes it more convenient for reutilization and friendly to the environment.

Wang reported the successful preparation of a Mg-based luminescent MIL-53 MOF.[66] Desolvated, this framework can be used as an absorbent for selective adsorption and separation of liquid explosives, including nitroaromatic (nitrobenzene (NB)) and nitroaliphatic (nitromethane (NM) and nitroethane (NE)) compounds, through single crystal-to-single crystal (SC–SC) transformations. On the basis of single crystal analysis, Wang provided direct evidence that both the selective adsorption and fluorescence quenching of the desolvated compound **1a** are dictated by host-guest interactions between guest liquid explosives and the host framework. Such findings differ from those reported in previous studies, which were dominated by surficial close contact interactions (Fig. 14).

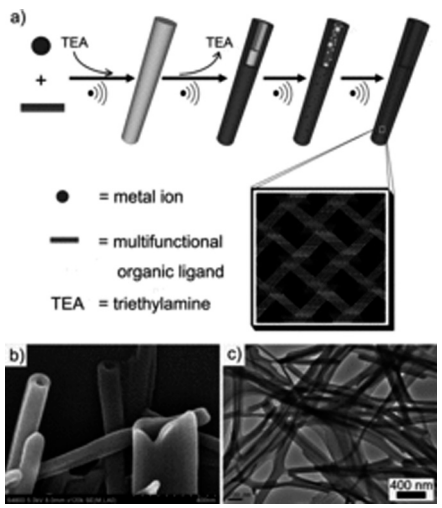

Fig. 12 (a) Illustration of the fabrication process of MOFNTs by the self-sacrificing template strategy. (b) Close-up SEM image of open-ended MOFNTs. (c) Representative TEM image of MOFNTs. Reprinted with permission from ref. 81. Copyright the Royal Society of Chemistry 2014.

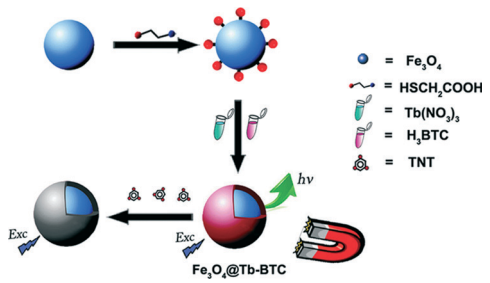

Fig. 13 Schematic of the fabrication process of Fe_3O_4@Tb-BTC nanospheres. Reprinted with permission from ref. 82. Copyright the Royal Society of Chemistry 2014.

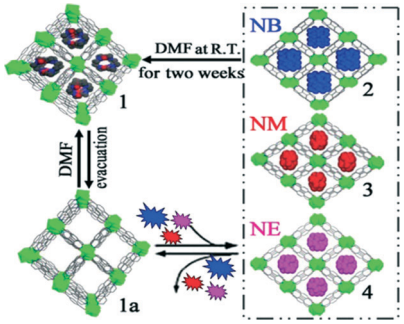

Fig. 14 Perspective views of the 3D open framework with 1D channel in 1 (with guest DMF molecules) and desolvated 1a; reversibly selective adsorption of NB (2, in blue), NM (3, in red) and NE (4, in purple) by 1a; crystals of 1 could be regenerated from 2, 3 and 4 by soaking them in DMF for two weeks at room temperature. Color code for 1: green, Mg; red, O; blue, N; 50% gray, C. Reprinted with permission from ref. 66. Copyright the Royal Society of Chemistry 2014.

Mukherjee and coworkers reported three electron-rich MOFs by employing ligands bearing aromatic tags.[27] The key role of the chosen aromatic tags is to enhance the π-electron density of the luminescent MOFs. The study has revealed that all these three prepared MOFs exhibited high selectivity towards explosive nitroaromatics, such as DNT, TNT, and TNB, over the other electron-deficient aromatics.

3. MOF Film for the NACs sensor

Many signal transduction schemes require a physical interface between the MOF and a device. This generally involves fabricating the MOF as a thin film on a surface. The increasing interest in utilizing MOFs as sensors or as selective membranes has led to a surge of interest in preparing MOF thin films.[8a,10]

Most commonly, MOF films have been synthesized directly on the surface of interest from the appropriate molecular and ionic precursors. Typically, the surface is a metal, metal oxide, glass, or silicon. Film formation can sometimes be accomplished by simply placing a platform in a reactor with the MOF precursors. These direct growth approaches often require functionalization of the surface with a self-assembled monolayer or seeding of the growth with small MOF crystals to nucleate film formation. In some cases, MOF films can be grown one molecular or ionic layer at a time by sequential immersions in solutions of the metal and organic precursors.[10] These synthetic methods are typically multiple-step and time-consuming. Moreover, the substrate surfaces in these synthetic procedures need to be either electro-statically compatible or chemically modified upon pretreatment. Fransaer and co-workers reported the flexibility of the electrochemical synthesis of MOFs films is illustrated by the preparation of well-adhering layers of luminescent MOFs on electrically conductive solid substrates.[83] The luminescent layers have been successfully tested for the detection of 2,4-dinitrotoluene (DNT). Similarly, a facile electrochemical plating method by means of applying voltage onto zinc electrodes in a BTC electrolyte has been developed to prepare fluorescent MOF films ($Zn_3(BTC)_2$) (Fig. 15).[84] Voltage and fabrication time are found to be the key parameters for the formation and morphology control of MOF films. In addition, the as-prepared MOF films, due to their evident fluorescence, are explored for potential applications in detecting nitro explosives with detection limit as low as 0.5 ppm. The fluorescent MOF films can be further applied to distinguish nitro explosives by varying the solution concentration. Moreover, the MOF films exhibit excellent reusability in consecutive nitro explosive detection reactions.

A second method for film fabrication is to first synthesize MOF particles and then mix them with other materials to obtain film. This has been demonstrated, for example, in Wen's study: thin films of Zn-MOF/PST-1 with a macroporous network structure were prepared using an electrospinning technique.[85] The secondary growth technique was developed to strongly anchor Zn-MOF seed crystals on porous supports Zn-MOF/PST-1 to form Zn-MOF/PST-2 thin films. The MOF films of secondary growth have a good fluorescence quenching sensitivity to nitroaromatic explosives, such as dinitrotoluene (DNT) and 2,4,6-trinitrotoluene (TNT), and thus can be good candidates for the detection of trace nitroaromatic explosives.

Jaworski and Jung reported that nanocomposites containing azobenzoic acid-functionalized graphene oxide and *trans*-4,4′-stilbene dicarboxylic acid in the presence of Zn^{2+} have been prepared with various ratios of the two components.[86] As shown in Fig. 16, the structure of the precursors is preserved in the composites, where graphene layers

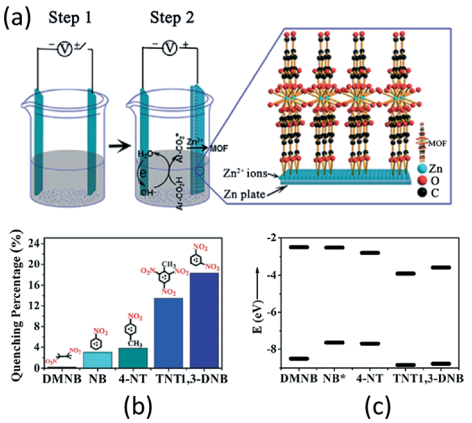

Fig. 15 (a) Schematic of the preparation procedure of $Zn_3(BTC)_2$ MOF films; (b) quenching percentage of MOF films for different nitro explosive detection methods (0.5 ppm) in ethanol (excited and monitored at 327 nm and 362 nm, respectively); (c) theoretical HOMO and LUMO energies for some nitro explosives. Reprinted with permission from ref. 84. Copyright the Royal Society of Chemistry 2014.

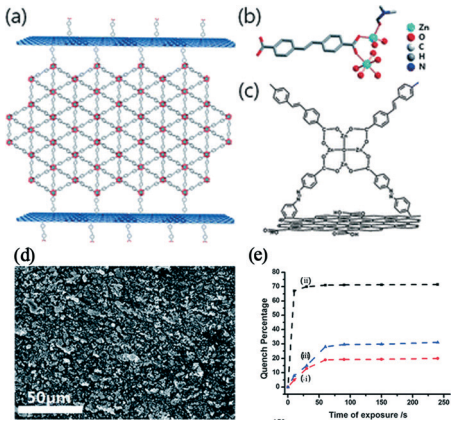

Fig. 16 (a) Schematic of the proposed bonding between L–Zn^{2+} and A-GO–Zn^{2+}. (b) The crystal structure of L–Zn^{2+} showed two different coordination environments, which have octahedral and tetrahedral coordination. (c) Its simplified version. (d) Top view of SEM images of nanocomposite 1 layer of A-GO/L–Zn^{2+}. (e) Fluorescence quenching of nanocomposite of A-GO/L–Zn^{2+} when exposed to (i) TNT and (ii) DNT vapors; (iii) fluorescence quenching of pure crystal L–Zn^{2+} when exposed to DNT vapor. Reprinted with permission from ref. 86. Copyright the Royal Society of Chemistry 2013.

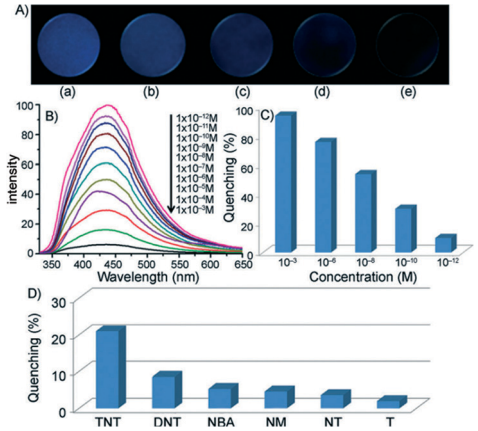

Fig. 17 (A) Images of the fluorescence quenching of gel 1-Zn^{2+}-coated test strips by different concentrations of TNT; (a) 0 M, (b) 1.0×10^{-12} M, (c) 1.0×10^{-10} M, (d) 1.0×10^{-8} M, and (e) 1.0×10^{-6} M; (B) Fluorescence spectral changes of the test strips on contact with added amount of TNT (λ_{ex} = 302 nm); (C) plot of the quenching (%) against concentration of added TNT in acetonitrile; (D) contact-mode detection of the lowest amount of different analytes (1.0×10^{-12} M) by the emission quenching test strip. Reprinted with permission from ref. 87. Copyright Wiley 2013.

from A-GO alternate with layers of MOF structures. The nanocomposites can act as chemosensors for the detection of DNT molecules.

An unusual, but useful, third approach involves MOF film formation within the spatial constraints of a gel layer. Lee and Jung reported on the use of a fluorescent MOF hydrogel that exhibits a higher detection capability for TNT in the gel state compared with that in the solution state (Fig. 17).[87] A portable sensor prepared from filter paper coated by the hydrogel was able to detect TNT at the pictogram level with a detection limit of 1.82 ppt (parts per trillion). It presents a simple and new means to provide selective detection of TNT on a surface or in an aqueous solution, as afforded by the unique molecular packing through the MOF structure in the gel formation and the associated photophysical properties.

4. Conclusions

In summary, we have briefly reviewed the recent research that is ongoing in the field of LMOFs for sensing NACs, including possible mechanisms for sensing. MOFs are intrinsic candidates for sensing due to their luminescent and porous qualities, in which water-stable LMOFs for NACs sensing is a potential development direction because of the protection of the environment and practical applications. As one of the most important parts of MOFs, it is supposed that the choice of metal ions is also worth discussing. Zn, Na, Mg and Zr ions can be exploited widely instead of Cd and Ni ions. Hundreds of studies have been reported about LMOFs for NACs sensing, but the study of LMOFs is a new research area. As for NACs, more clear and simple signal changes can be obtained, such as color changes in the range of visible light and "naked-eye" detection. The advantage of LMOFs can also be taken through post-modification or by composite with other materials. At the same time, it is much appreciated that preparing the device using stable and efficient MOF material makes the detection process simpler and easier. Moreover, it will be an important step in the development process of MOF materials in the detection of NACs.

List of abbreviations

2,4-DNT	2,4-Dinitrotoluene
2,6-DNT	2,6-Dinitrotoluene
H_3BTC	1,3,5-Benzenetricarboxylic acid
H_3CPEIP	5-((4-Carboxyphenyl)ethynyl)isophthalic acid
HDMA	Protonated dimethylamine cations
H_2L^1	5-(Benzyloxy)isophthalic acid
H_2L^2	5-(Naphthalen-1-ylmethoxy)isophthalic acid
H_2L^3	5-(Pyren-1-ylmethoxy)isophthalic acid
H_4L^4	Bis-(3,5-dicarboxy-phenyl)terephthalamide
H_4L^5	1,1′-Biphenyl-2,3,3′,5′-tetracarboxylic acid
H_2L^6	3,3′-Dimethoxybiphenyl-4,4′-dicarboxylic acid
H_3L^7	1,3,5-Tris(4-carboxyphenyl-1-ylmethyl)-2,4,6-trimethylbenzene
H_8L^8	2,8,14,20-Tetra-methyl-4,6,10,12,16,18,22,24-octa-carboxymethoxy-calix[4]arene
$H_{12}L^9$	[[5,5′,5″,5‴,5],5]′-[1,2,3,4,5,6-Phenylhexamethoxyl]hexaisophthalic acid
H_3L^{10}	2,4,6-Tris[1-(3-carboxylphenoxy)ylmethyl]mesitylene
H_2L^{11}	9,9-Diethylfluorene-2,7-dicarboxylic acid
H_8L^{12}	Tetrakis[(3,5-dicarboxyphenoxy)methyl]methane
H_2L^{13}	3,3′-(Thiophene-2,5-diyl)dibenzoic acid
H_4L^{14}	1,1′-(1,4-Phenylenebis(methylene))bis(1*H*-pyrazole-3,5-dicarboxylic acid)
H_4L^{15}	[1,1′:4′,1″-Terphenyl]-2′,3,3″,5′-tetracarboxylicacid
H_3L^{16}	4,4′,4″-((2,2′,2″-(Nitrilotris(methylene))tris(1*H*-benzo[*d*]imidazole-2,1-diyl)(tris(methylene))tribenzoic acid
H_3L^{17}	4,4′,4″-((2,2′,2″-(Nitrilotris(methylene))tris(1*H*-benzo[*d*]-imidazole-2,1-diyl))tris(methylene))tribenzoic acid
H_4L^{18}	Bis-(3,5-dicarboxy-phenyl)terephthalamide
H_3L^{19}	1,3,5-Tri(4-carboxyphenoxy)benzene
H_2L^{20}	2-(2-Hydroxy-propionylamino)-terephthalic acid
H_2L^{21}	5-(4-Carboxyphenyl)pyridine-2-carboxylate
H_2L^{22}	2′-Amino-[1,1′:4′,1″-terphenyl]-4,4″-dicarboxylic acid
H_2L^{24}	2-Phenylpyridine-5,4′-dicarboxylic acid
H_2bpdc	4,4′-Biphenyldicarboxylic acid
H_4BPTA	[1,1′-Biphenyl]-2,2′,5,5′-tetracarboxylic acid
H_3BTB	1,3,5-Benzenetrisbenzoic acid
H_4BTEC	1,2,4,5-Benzenetetracarboxylic acid
H_2CPMA	Bis(4-carboxyphenyl)-*N*-methylamine
H_2DCPB	1,3-Di(4-carboxyphenyl)benzene
Hdmpp	3,5-Dimethyl-4-(4′-pyridyl)pyrazole
H_2MFDA	9,9-Dimethyl-fluorene-2,7-dicarboxylic acid
H3NTB	4,4′,4″-Nitrilotrisbenzoic acid

H_2oba	4,4′-Oxybis(benzoic acid)
H_2PIA	5-(Pyridine-4-yl)isophthalic acid
Htba	4-(1*H*-1,2,4-Triazol-1-yl)benzoic acid
H_4TCPPE	Tetrakis[4-(4-carboxyphenyl)phenyl]ethene
H_3TPT	*p*-Terphenyl-3,4″,5-tricarboxylic acid
H_4ttac	1,1′,2′,1″-Terphenyl-4,4′,4″,5′-tetracarboxylic acid
H_3TTCA	Triphenylene-2,6,10-tricarboxylic acid
H_3TTPB	1,3,5-Tri(4-(2*H*-tetrazol-5-yl)phenoxy)benzene
ad	Adenine
BDC	Benzene-1,4-dicarboxylate
bimb	4,4′-Bis(1-imidazolyl)biphenyl
bpe	1,2-Bis(4-pyridyl)-ethane
bpeb	1,4-Bis[2-(4′-pyridyl)ethenyl]benzene
bpee	1,2-Bis(4-pyridyl)ethylene
BPNO	4,4′-Dipyridyl-*N*,*N*′-dioxide
bpp	1,3-Bis(4-pyridyl)propane
BPTC	Biphenyl-3,3′,5,5′-tetracarboxylic acid
bpy	4,4′-Bipyridine
bpydbH_2	4,4′-(4,4′-Bipyridine-2,6-diyl)dibenzoic acid
dcbpy	2,2′-Bipyridine-4,40-dicarboxylate
DEF	*N*,*N*′-Diethylformamide
D-H_2cam	D-camphor acid
Diox	1,4-Dioxane
dipb	4,4′-Di(1*H*-imidazol-1-yl)-1,10-biphenyl
DMA	*N*,*N*′-Dimethylacetamide
DMF	*N*,*N*′-Dimethylformamide
DMSO	Dimethyl sulphoxide
dpb	1,4-Di(4-pyridyl)benzene
dpe	1,2-Di(4-pyridyl)ethylene
dpyb	1,4-Di(pyridin-4-yl)benzene
en	1,2-Ethanediamine
fdc	2,5-Furandicarboxylatedianion
IPA	Isophthalic acid
G	Guest solvent molecules
L^{23}	4′-(4-Methoxyphenyl)-4,2′:6′,4″-terpyridine
m-DNB	1,3-Dinitrobenzene
NB	Nitrobenzene
NDC	2,6-Naphthalenedicarboxylic acid
NMP	1-Methyl-2-pyrrolidone
NT	2-Nitrotoluene
PA	Picric acid
PAM	4,4′-Methylenebis(3-hydroxy-2-naphthalenecarboxylate)
PCA	4-Pyridinecaboxylicacid
p-DNB	1,4-dinitrobenzene
ppvppa	*N*-(Pyridin-2-yl)-*N*-(4-(2-(pyridin-4-yl)vinyl)phenyl)-pyridin-2-amine
PPZ	Piperazine
sdb	4,4′-Sulfonyldibenzoate
TATAB	4,4′,4″-*s*-Triazine-1,3,5-triyltri-p-aminobenzoate
TCA	Tri-carboxytriphenylamine
TDPAT	2,4,6-Tris(3,5-dicarboxylphenylamino)-1,3,5-triazine
ted	Triethylenediamine
TNT	2,4,6-Trinitrotoluene
TPTZ	{4-[4-(1*H*-1,2,4-Triazol-1-yl)phenyl]phenyl}-1*H*-1,2,4-triazole

Acknowledgements

This study was financially supported by the NSFC (Grant No. 21371179, 21271117 and 21571187), NCET-11-0309, the Shandong Natural Science Fund for Distinguished Young Scholars (JQ201003), and the Fundamental Research Funds for the Central Universities (13CX05010A, 14CX02150A, 14CX02158A).

Notes and references

1 (*a*) S. W. Thomas III, G. D. Joly and T. M. Swager, *Chem. Rev.*, 2007, **107**, 1339–1386; (*b*) D. T. McQuade, A. E. Pullen and T. M. Swager, *Chem. Rev.*, 2010, **100**, 2537–2574; (*c*) A. Lan, K. Li, H. Wu, D. H. Olson, T. J. Emge, W. Ki, M. Hong and J. Li, *Angew. Chem., Int. Ed.*, 2009, **48**, 2334–2338; (*d*) M. E. Germain and M. J. Knapp, *Chem. Soc. Rev.*, 2009, **38**, 2543–2555; (*e*) Y. Salinas, R. Martinez-Manez, M. D. Marcos, F. Sancenon, A. M. Costero, M. Parra and S. Gil, *Chem. Soc. Rev.*, 2012, **41**, 1261–1296; (*f*) D. Banerjee, Z. Hu and J. Li, *Dalton Trans.*, 2014, **43**, 10668–10685; (*g*) S. Pramanik, C. Zheng, X. Zhang, T. J. Emge and J. Li, *J. Am. Chem. Soc.*, 2011, **133**, 4153–4155; (*h*) B. Liu, *J. Mater. Chem.*, 2012, **22**, 10094–10101; (*i*) S. J. Toal and W. C. Trogler, *J. Mater. Chem.*, 2006, **16**, 2871–2883; (*j*) L. Senesac and T. G. Thundat, *Mater. Today*, 2008, **11**, 28–36; (*k*) D. S. Moore, *Rev. Sci. Instrum.*, 2004, **75**, 2499–2512; (*l*) W. Wang, J. Yang, R. Wang, L. Zhang, J. Yu and D. Sun, *Cryst. Growth Des.*, 2015, **15**, 2589–2592; (*m*) K. S. Asha, K. Bhattacharyyab and S. Mandal, *J. Mater. Chem. C*, 2014, **2**, 10073–10081.

2 S. Shanmugaraju and P. S. Mukherjee, *Chem. – Eur. J.*, 2015, **21**, 6656–6666.

3 (*a*) Z. Hu, B. J. Deibert and J. Li, *Chem. Soc. Rev.*, 2014, **43**, 5815–5840; (*b*) M.-M. Chen, X. Zhou, H.-X. Li, X.-X. Yang and J.-P. Lang, *Cryst. Growth Des.*, 2015, **15**, 2753–2760; (*c*) L. Liu, X. F. Chen, J. S. Qiu and C. Hao, *Dalton Trans.*, 2015, **44**, 2897–2906.

4 (*a*) V. P. Anferov, G. V. Mozjoukhine and R. Fisher, *Rev. Sci. Instrum.*, 2000, **71**, 1656–1659; (*b*) J. M. Sylvia, J. A. Janni, J. D. Klein and K. M. Spencer, *Anal. Chem.*, 2000, **72**, 5834–5840; (*c*) K. Hakansson, R. V. Coorey, R. A. Zubarev, V. L. Talrose and P. Hakansson, *J. Mass Spectrom.*, 2000, **35**, 337–346; (*d*) S. F. Hallowell, *Talanta*, 2001, **54**, 447–458; (*e*) G. A. Eiceman and J. A. Stone, *Anal. Chem.*, 2004, **76**, 390A–397A; (*f*) Z. Takats, I. Cotte-Rodriguez, N. Talaty, H. Chen and R. G. Cooks, *Chem. Commun.*, 2005, 1950–1952; (*g*) R. D. Luggar, M. J. Farquharson, J. A. Horrocks and R. J. Lacey, *X-Ray Spectrom.*, 1998, **27**, 87–94.

5 (*a*) S. Rochat and T. M. Swager, *ACS Appl. Mater. Interfaces*, 2013, **5**, 4488–4502; (*b*) J. C. Sanchez and W. C. Trogler, *J. Mater. Chem.*, 2008, **18**, 3143–3156.

6 (*a*) M. P. Suh, H. J. Park, T. K. Prasad and D. Lim, *Chem. Rev.*, 2012, **112**, 782–835; (*b*) R. B. Getman, Y. S. Bae, C. E. Wilmer and R. Q. Snurr, *Chem. Rev.*, 2012, **112**, 703–723; (*c*) J. R. Li, J. Sculley and H. C. Zhou, *Chem. Rev.*, 2012, **112**, 869–932; (*d*) K. Sumida, D. L. Rogow, J. A. Mason, T. M. McDonald, E. D. Bloch, Z. R. Herm, T. H. Bae and J. R. Long,

Chem. Rev., 2012, **112**, 724–781; (*e*) Y. He, W. Zhou, G. Qian and B. Chen, *Chem. Soc. Rev.*, 2014, **43**, 5657–5678; (*f*) J. R. Li, R. J. Kuppler and H. C. Zhou, *Chem. Soc. Rev.*, 2009, **38**, 1477–1504; (*g*) B. Van de Voorde, B. Bueken, J. Denayer and D. De Vos, *Chem. Soc. Rev.*, 2014, **43**, 5766–5788.

7 (*a*) L. Ma, C. Abney and W. Lin, *Chem. Soc. Rev.*, 2009, **38**, 1248–1256; (*b*) M. Zhao, S. Ou and C. D. Wu, *Acc. Chem. Res.*, 2014, **47**, 1199–1207; (*c*) A. Dhakshinamoorthy and H. Garcia, *Chem. Soc. Rev.*, 2014, **43**, 5750–5765; (*d*) J. Lee, O. K. Farha, J. Roberts, K. A. Scheidt, S. T. Nguyen and J. T. Hupp, *Chem. Soc. Rev.*, 2009, **38**, 1450–1459; (*e*) J. Liu, L. Chen, H. Cui, J. Zhang, L. Zhang and C. Y. Su, *Chem. Soc. Rev.*, 2014, **43**, 6011–6061.

8 (*a*) L. E. Kreno, K. Leong, O. K. Farha, M. Allendorf, R. P. Van Duyne and J. T. Hupp, *Chem. Rev.*, 2012, **112**, 1105–1125; (*b*) Y. Cui, Y. Yue, G. Qian and B. Chen, *Chem. Rev.*, 2012, **112**, 1126–1162; (*c*) J. Rocha, L. D. Carlos, F. A. Paz and D. Ananias, *Chem. Soc. Rev.*, 2011, **40**, 926–940; (*d*) Y. Cui, B. Chen and G. Qian, *Coord. Chem. Rev.*, 2014, 76–86.

9 R. C. Huxford, J. D. Rocca and W. Lin, *Curr. Opin. Chem. Biol.*, 2010, **14**, 262–268.

10 (*a*) H.-L. Jiang, T. A. Makal and H.-C. Zhou, *Coord. Chem. Rev.*, 2013, **257**, 2232–2249; (*b*) Y. Chen, G. Li, Z. Chang, Y. Qu, Y. Zhang and X. Bu, *Chem. Sci.*, 2013, **4**, 3678–3682; (*c*) Y. Li, J. Li, L. Wang, B. Zhou, Q. Chen and X. Bu, *J. Mater. Chem. A*, 2013, **1**, 495–499.

11 K. Müller-Buschbaum, F. Beuerle and C. Feldmann, *Microporous Mesoporous Mater.*, 2015, **216**, 171–199.

12 (*a*) S. S. Nagarkar, B. Joarder, A. K. Chaudhari, S. Mukherjee and S. K. Ghosh, *Angew. Chem., Int. Ed.*, 2013, **52**, 2881–2885; (*b*) J. R. Lakowicz, *Principles of Florescence spectroscopy*, Springer, Singapore, 3rd edn, 2010.

13 G. V. Zyryanov, D. S. Kopchuk, I. S. Kovalev, E. V. Nosova, V. L. Rusinov and O. N. Chupakhin, *Russ. Chem. Rev.*, 2014, **83**, 783–819.

14 B. Gole, A. K. Bar and P. S. Mukherjee, *Chem. – Eur. J.*, 2014, **20**, 2276–2291.

15 G.-Y. Wang, C. Song, D.-M. Kong, W.-J. Ruan, Z. Chang and Y. Li, *J. Mater. Chem. A*, 2014, **2**, 2213–2220.

16 Q. Zhang, A. Geng, H. Zhang, F. Hu, Z. H. Lu, D. Sun, X. Wei and C. Ma, *Chem. – Eur. J.*, 2014, **20**, 4885–4890.

17 D. Singh and C. M. Nagaraja, *Cryst. Growth Des.*, 2015, **15**, 3356–3365.

18 L. Sun, H. Xing, J. Xu, Z. Liang, J. Yu and R. Xu, *Dalton Trans.*, 2013, **42**, 5508–5513.

19 A.-X. Zhu, Z.-Z. Qiu, L.-B. Yang, X.-D. Fang, S.-J. Chen, Q.-Q. Xu and Q.-X. Li, *CrystEngComm*, 2015, **17**, 4787–4792.

20 C. Q. Zhang, Y. Yan, J. Y. Li, X. W. Song, Y. L. Liu and Z. Q. Liang, *Dalton Trans.*, 2015, **44**, 230–236.

21 C. Q. Zhang, Y. Yan, Q. H. Pan, L. B. Sun, H. M. He, Y. L. Liu, Z. Q. Liang and J. Y. Li, *Dalton Trans.*, 2015, **44**, 13340–13346.

22 H. Xu, F. Liu, Y. Cui, B. Chen and G. Qian, *Chem. Commun.*, 2011, **47**, 3153–3155.

23 W. Sun, J. Wang, H. Liu, S. Chang, X. Qin and Z. Liu, *Mater. Lett.*, 2014, **126**, 189–192.

24 H. Zhang, D. M. Chen, H. L. Ma and P. Cheng, *Chem. – Eur. J.*, 2015, **21**, 15854–15859.

25 J.-D. Xiao, L.-G. Qiu, F. Ke, Y.-P. Yuan, G.-S. Xu, Y.-M. Wang and X. Jiang, *J. Mater. Chem. A*, 2013, **1**, 8745–8752.

26 Y. N. Gong, L. Jiang and T. B. Lu, *Chem. Commun.*, 2013, **49**, 11113–11115.

27 B. Gole, A. K. Bar and P. S. Mukherjee, *Chem. – Eur. J.*, 2014, **20**, 13321–13336.

28 D. X. Ma, B. Y. Li, X. J. Zhou, Q. Zhou, K. Liu, G. Zeng, G. H. Li, Z. Shi and S. H. Feng, *Chem. Commun.*, 2013, **49**, 8964–8966.

29 Z. Zhang, S. Xiang, X. Rao, Q. Zheng, F. R. Fronczek, G. Qian and B. Chen, *Chem. Commun.*, 2010, **46**, 7205–7207.

30 Y. Kim, J. H. Song, W. R. Lee, W. J. Phang, K. S. Lim and C. S. Hong, *Cryst. Growth Des.*, 2014, **14**, 1933–1937.

31 Y. N. Gong, Y. L. Huang, L. Jiang and T. B. Lu, *Inorg. Chem.*, 2014, **53**, 9457–9459.

32 J. Ye, X. Wang, R. F. Bogale, L. Zhao, H. Cheng, W. Gong, J. Zhao and G. Ning, *Sens. Actuators, B*, 2015, **210**, 566–573.

33 J. Ye, L. Zhao, R. F. Bogale, Y. Gao, X. Wang, X. Qian, S. Guo, J. Zhao and G. Ning, *Chem. – Eur. J.*, 2015, **21**, 2029–2037.

34 X. Q. Wang, L. L. Zhang, J. Yang, F. L. Liu, F. N. Dai, R. M. Wang and D. F. Sun, *J. Mater. Chem. A*, 2015, **3**, 12777–12785.

35 T. K. Kim, J. H. Lee, D. Moon and H. R. Moon, *Inorg. Chem.*, 2013, **52**, 589–595.

36 Z.-F. Wu, B. Tan, M.-L. Feng, C.-F. Du and X.-Y. Huang, *J. Solid State Chem.*, 2015, **223**, 59–64.

37 Q. Zheng, F. Yang, M. Deng, Y. Ling, X. Liu, Z. Chen, Y. Wang, L. Weng and Y. Zhou, *Inorg. Chem.*, 2013, **52**, 10368–10374.

38 I. H. Park, R. Medishetty, J. Y. Kim, S. S. Lee and J. J. Vittal, *Angew. Chem., Int. Ed.*, 2014, **53**, 5591–5595.

39 D. Singh and C. M. Nagaraja, *Dalton Trans.*, 2014, **43**, 17912–17915.

40 H. He, Y. Song, F. Sun, Z. Bian, L. Gao and G. Zhu, *J. Mater. Chem. A*, 2015, **3**, 16598–16603.

41 H. Zhang, W. Jiang, J. Yang, Y.-Y. Liu, S. Song and J.-F. Ma, *CrystEngComm*, 2014, **16**, 9939–9946.

42 Y. C. He, H. M. Zhang, Y. Y. Liu, Q. Y. Zhai, Q. T. Shen, S. Y. Song and J. F. Ma, *Cryst. Growth Des.*, 2014, **14**, 3174–3178.

43 M. Venkateswarulu, A. Pramanik and R. R. Koner, *Dalton Trans.*, 2015, **44**, 6348–6352.

44 D. Tian, Y. Li, R.-Y. Chen, Z. Chang, G.-Y. Wang and X.-H. Bu, *J. Mater. Chem. A*, 2014, **2**, 1465–1470.

45 L. L. Wen, X. Y. Xu, K. L. Lv, Y. M. Huang, X. F. Zheng, L. Zhou, R. Q. Sun and D. F. Li, *ACS Appl. Mater. Interfaces*, 2015, **7**, 4449–4455.

46 Y. Wang, L. Cheng, Z. Y. Liu, X. G. Wang, B. Ding, L. Yin, B. B. Zhou, M. S. Li, J. X. Wang and X. J. Zhao, *Chem. – Eur. J.*, 2015, **21**, 14171–14178.

47 H. He, Y. Song, F. Sun, N. Zhao and G. Zhu, *Cryst. Growth Des.*, 2015, **15**, 2033–2038.

48 D. Tian, R.-Y. Chen, J. Xu, Y.-W. Li and X.-H. Bu, *APL Mater.*, 2014, **2**, 124111–124117.

49 X. Zhou, H. Li, H. Xiao, L. Li, Q. Zhao, T. Yang, J. Zuo and W. Huang, *Dalton Trans.*, 2013, **42**, 5718–5723.
50 A. Li, L. Li, Z. Lin, L. Song, Z. H. Wang, Q. Chen, T. Yang, X. H. Zhou, H. P. Xiao and X. J. Yin, *New J. Chem.*, 2015, **39**, 2289–2295.
51 X. H. Zhou, L. Li, H. H. Li, A. Li, T. Yang and W. Huang, *Dalton Trans.*, 2013, **42**, 12403–12409.
52 S.-N. Zhao, X.-Z. Song, M. Zhu, X. Meng, L.-L. Wu, S.-Y. Song, C. Wang and H.-J. Zhang, *RSC Adv.*, 2015, **5**, 93–98.
53 Y.-S. Xue, Y. He, L. Zhou, F.-J. Chen, Y. Xu, H.-B. Du, X.-Z. You and B. Chen, *J. Mater. Chem. A*, 2013, **1**, 4525–4530.
54 Z.-F. Wu, B. Tan, M.-L. Feng, A.-J. Lan and X.-Y. Huang, *J. Mater. Chem. A*, 2014, **2**, 6426–6431.
55 Z. W. J. Yang, K. L. Hu, Y. S. Li, J. F. Feng, J. L. Shi and J. L. Gu, *ACS Appl. Mater. Interfaces*, 2015, **7**, 11956–11964.
56 Z. Q. Shi, Z. J. Guo and H. G. Zheng, *Chem. Commun.*, 2015, **51**, 8300–8303.
57 Y.-P. Xia, Y.-W. Li, D.-C. Li, Q.-X. Yao, Y.-C. Du and J.-M. Dou, *CrystEngComm*, 2015, **17**, 2459–2463.
58 Y. Wu, G.-P. Yang, Y. Zhao, W.-P. Wu, B. Liu and Y.-Y. Wang, *Dalton Trans.*, 2015, **44**, 3271–3277.
59 S. R. Zhang, D. Y. Du, J. S. Qin, S. J. Bao, S. L. Li, W. W. He, Y. Q. Lan, P. Shen and Z. M. Su, *Chem. – Eur. J.*, 2014, **20**, 3589–3594.
60 X. L. Hu, F. H. Liu, C. Qin, K. Z. Shao and Z. M. Su, *Dalton Trans.*, 2015, **44**, 7822–7827.
61 S. R. Zhang, D. Y. Du, J. S. Qin, S. L. Li, W. W. He, Y. Q. Lan and Z. M. Su, *Inorg. Chem.*, 2014, **53**, 8105–8113.
62 Y. Rachuri, B. Parmar, K. K. Bisht and E. Suresh, *Inorg. Chem. Front.*, 2015, **2**, 228–236.
63 X.-Z. Song, S.-Y. Song, S.-N. Zhao, Z.-M. Hao, M. Zhu, X. Meng, L.-L. Wu and H.-J. Zhang, *Adv. Funct. Mater.*, 2014, **24**, 4034–4041.
64 L.-Y. Pang, G.-P. Yang, J.-C. Jin, M. Kang, A.-Y. Fu, Y.-Y. Wang and Q.-Z. Shi, *Cryst. Growth Des.*, 2014, **14**, 2954–2961.
65 G. Y. Wang, L. L. Yang, Y. Li, H. Song, W. J. Ruan, Z. Chang and X. H. Bu, *Dalton Trans.*, 2013, **42**, 12865–12868.
66 Liu Dan, X. Liu, Y. Liu, Y. Yu, F. Chen and C. Wang, *Dalton Trans.*, 2014, **43**, 15237–15244.
67 A. K. Chaudhari, S. S. Nagarkar, B. Joarder and S. K. Ghosh, *Cryst. Growth Des.*, 2013, **13**, 3716–3721.
68 X. G. Liu, H. Wang, B. Chen, Y. Zou, Z. G. Gu, Z. Zhao and L. Shen, *Chem. Commun.*, 2015, **51**, 1677–1680.
69 D. Banerjee, Z. Hu, S. Pramanik, X. Zhang, H. Wang and J. Li, *CrystEngComm*, 2013, **15**, 9745–9750.
70 M. Jurcic, W. J. Peveler, C. N. Savory, D. O. Scanlon, A. J. Kenyone and I. P. Parkin, *J. Mater. Chem. A*, 2015, **3**, 6351–6359.
71 B. Joarder, A. V. Desai, P. Samanta, S. Mukherjee and S. K. Ghosh, *Chem. – Eur. J.*, 2015, **21**, 965–969.
72 E.-L. Zhou, P. Huang, C. Qin, K.-Z. Shao and Z.-M. Su, *J. Mater. Chem. A*, 2015, **3**, 7224–7228.
73 J. H. Qin, B. Ma, X. F. Liu, H. L. Lu, X. Y. Dong, S. Q. Zang and H. W. Hou, *Dalton Trans.*, 2015, **44**, 14594–14603.
74 L.-H. Cao, F. Shi, W.-M. Zhang, S.-Q. Zang and T. C. W. Mak, *Chem. – Eur. J.*, 2015, **21**, 15705–15712.
75 J. H. Qin, B. Ma, X. F. Liu, H. L. Lu, X. Y. Dong, S. Q. Zang and H. W. Hou, *J. Mater. Chem. A*, 2015, **3**, 12690–12697.
76 S. S. Nagarkar, A. V. Desai, P. Samanta and S. K. Ghosh, *Dalton Trans.*, 2015, **44**, 15175–15180.
77 S. S. Nagarkar, A. V. Desai and S. K. Ghosh, *Chem. Commun.*, 2014, **50**, 8915–8918.
78 S. Mukherjee, A. V. Desai, B. Manna, A. I. Inamdar and S. K. Ghosh, *Cryst. Growth Des.*, 2015, **15**, 4627–4634.
79 W. Xie, S. R. Zhang, D. Y. Du, J. S. Qin, S. J. Bao, J. Li, Z. M. Su, W. W. He, Q. Fu and Y. Q. Lan, *Inorg. Chem.*, 2015, **54**, 3290–3296.
80 S. Khatua, S. Goswami, S. Biswas, K. Tomar, H. S. Jena and S. Konar, *Chem. Mater.*, 2015, **27**, 5349–5360.
81 R. Li, Y. P. Yuan, L. G. Qiu, W. Zhang and J. F. Zhu, *Small*, 2012, **8**, 225–230.
82 J. J. Qian, L. G. Qiu, Y. M. Wang, Y. P. Yuan, A. J. Xie and Y. H. Shen, *Dalton Trans.*, 2014, **43**, 3978–3983.
83 N. Campagnol, E. R. Souza, D. E. De Vos, K. Binnemans and J. Fransaer, *Chem. Commun.*, 2014, **50**, 12545–12547.
84 Y.-Y. Yang, Z.-J. Lin, T.-T. Liu, J. Liang and R. Cao, *CrystEngComm*, 2015, **17**, 1381–1388.
85 Y. Xu, Y. Wen, W. Zhu, Y.-N. Wu, C. Lin and G. Li, *Mater. Lett.*, 2012, **87**, 20–23.
86 J. H. Lee, J. Jaworski and J. H. Jung, *Nanoscale*, 2013, **5**, 8533–8540.
87 J. H. Lee, S. Kang, J. Y. Lee, J. Jaworski and J. H. Jung, *Chem. – Eur. J.*, 2013, **19**, 16665–16671.

